Yao *et al.*
Protection and Control of Modern Power Systems (2023) 8:9
https://doi.org/10.1186/s41601-023-00282-1

Protection and Control of Modern Power Systems

ORIGINAL RESEARCH Open Access

A high efficiency multi-module parallel RF inverter system for plasma induced hydrogen

Tingting Yao, Yueshi Guan* and Wei Wang

Abstract

Hydrogen energy plays an important role in achieving carbon neutralization, and plasma induced hydrogen is an effective production method. One challenge is how to guarantee high efficiency operation with wide power output range of the RF inverter system used to generate the plasma. In this paper, a multi-module parallel topology of a high-frequency inverter is analyzed, in which the power combining network can maintain the soft switching characteristics of the inverter modules. A control method of "ON/OFF + phase shift" is adopted to broaden the output power range of the inverter. The equivalent impedances of different modules are analyzed in detail. A four-module 13.56 MHz high-frequency inverter prototype is built and tested. The results show that the inverter can operate at high efficiency and wide output power range with efficiency improved by at least 5% compared with the traditional parameter design method without considering the effect of paralleled modules.

Keywords High-frequency inverter, Multi-module parallel connection, Wide power range

1 Introduction

With the fast development of clean energy, hydrogen energy has an important role in achieving carbon neutralization. Plasma-induced hydrogen is an effective method of hydrogen production [1–6]. The plasma is usually generated by an RF inverter system, which is required to generate RF output with high frequency, high speed and wide power range [7]. However, one challenge is that the RF inverter is very sensitive to output impedance so the output power range is limited for a single inverter.

At present, the output power of a single high-frequency inverter is limited by the switch voltage stress as well as acceptable efficiency, so modularization is needed to achieve wide power range and flexible output regulation. However, the interaction between modules can affect the equivalent impedance of the individual inverter module. Consequently, the output power of the RF inverter no longer varies linearly with the input voltage, resulting in complex or even uncertain power output. Furthermore, because the high-frequency inverter module is designed for a specific impedance, once the equivalent load changes, the characteristic of zero-voltage switching (ZVS) will be lost. As a result, the switching loss is greatly increased and system efficiency is significantly reduced [8–11]. These effects become more serious when multiple modules are used in the system.

The most traditional method is to use an isolated synthesizer to connect multiple modules. The isolated power synthesizer makes the equivalent impedance of each module constant, which can eliminate the interaction between modules and ensure the constant output power of each module. However, power that is not delivered to the output dissipates in the form of heat on the isolation resistor, resulting in an efficiency decrement of the inverter system. Another method is to use a non-isolated lossless power combination network. The most distinct synthesizers of this type are the Chireix synthesizer [12–14] and the Wilkinson synthesizer. In this form of connection, the equivalent impedance of a single inverter module changes with the phase shift angle and

*Correspondence:
Yueshi Guan
guanyueshi@hit.edu.cn
School of Electrical Engineering and Automation, Harbin Institute of Technology, Harbin, China

output power, and the conduction loss of the inverter decreases with the output power. When the phase shift angle increases, the reactive component of the equivalent impedance becomes very high, and the reactive power loss increases greatly. Therefore, some have proposed other non-isolated synthesizers with improved performance, such as the improved Chireix, multiplexing networks, etc. [15–17].

The adjustment of the output power is generally realized by the phase shift control between the modules. In order to further expand the range of power regulation, an input voltage control strategy is added in [18] on the basis of phase shift control. By setting a plurality of discrete input level values, the power regulation range is further improved. However, this topology needs to introduce additional hardware circuits to realize the adjustment of the input voltage level, and this greatly increases the complexity and volume of the system and reduces its power density. In addition, the difference in the input voltages will increase the difference between the various modules of the system. The voltage difference will cause a problem of parallel current sharing, making the analysis and design of the system more complicated. For systems with many modules, switching control of the modules can be added to further increase the range of power regulation [19]. This control does not require additional circuitry, but with switching and phase shifting control, the equivalent load of the module will change. At present, there is no relevant quantitative research to verify whether the soft switching characteristics of the system will be lost when switching and phase shift control is used, so further analysis and demonstration are needed where the low frequency inverter control can be used as guidance [20, 21].

In this paper, a multi-module high-frequency inverter system based on the Class E inverter is proposed, one which achieves impedance matching through the parameter design of the power connection network. Based on switching and phase shift control, the equivalent impedance of each inverter module of the system is quantitatively analyzed. In order to verify the theoretical analysis, a four-module high-frequency inverter system with the operating frequency of 13.56 MHz is built and tested.

2 Parameter design of multi-module inverter circuit

The multi-module inverter system analyzed in this paper is shown in Fig. 1. It is mainly composed of multiple parallel high-frequency inverter modules and a power connection network.

For the inverter modules, the performance of each module directly affects the efficiency of the system. When performing power regulation, the switching and phase

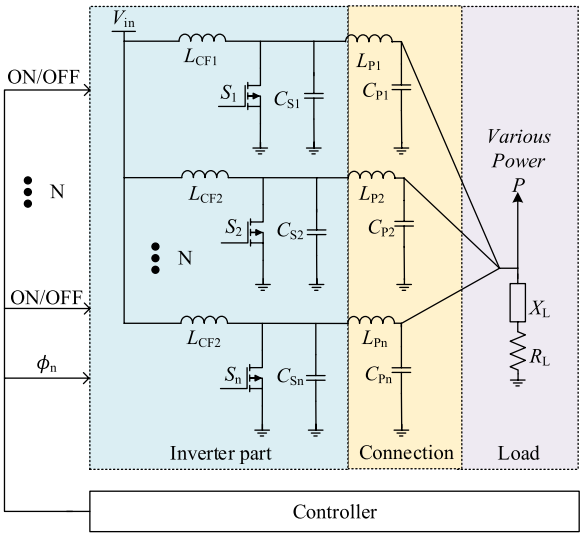

Fig. 1 Inverter system structure diagram

shift control of the system can be equivalent to a change in the impedance of the inverter. Since the efficiency of the resonant converter is sensitive to load changes, it is necessary to study the load impedance range corresponding to the efficient working area of each inverter module. For the power connection module, the addition of the connection network is expected to have no effect on the soft switching of the system.

2.1 Inverter module design

Given the design of a Class E inverter, the resonant inductance and capacitance can be calculated from (1), where x is an intermediate variable and is related only to the duty cycle D. When $D=0.5$, $x=4.5972$, and $f/f_s = 1.54$.

$$\begin{cases} L_{CF} = \dfrac{2R_L}{f_s} \cdot \dfrac{D^2(1-D)x\tan x + D[(1-D)\tan x]^2}{[(1-D)\tan x + Dx]^2 + (Dx\tan x)^2} \\ C_S = \dfrac{1}{2f_s \cdot R_L} \cdot \dfrac{D(1-D)\tan x}{Dx + (1-D)\tan x} \end{cases} \tag{1}$$

The high-efficiency operating range of the load network of a Class E inverter is analyzed here. The high-efficiency working area of high-frequency resonant converters is extremely narrow, and generally only ZVS and ZVDS can be realized at one specific load point at the same time. Ignoring the requirements for ZVDS, the drain-source voltage is allowed to drop to zero before the switch is turned on. Because of the existence of an anti-parallel diode across the actual switch tube, the negative drain-source voltage will be limited to − 0.7 V (almost zero), and thus ZVS can also be achieved.

The following is a quantitative analysis of the efficient operating load range of the Class E inverter. We start by making the following assumptions:

(1) Switch and diode are ideal and lossless devices.
(2) Capacitors C_S, C_F, inductor L_F and L_{CF} are linear and lossless, and their parasitic parameters such as ESR are not taken into account.
(4) The output current of the inverter is a sine wave, i.e., $i_O(\omega t)=I_O\sin(\omega t+\phi)$.
(5) We introduce the concept of normalized frequency, $A=f_s/f_{opt}$, and $A=1$ at rated frequency. When the duty cycle $D=0.5$, the rated load impedance $R_L=R_{nom}$.

The reactance of the shunt capacitor C_S at operating frequency f_s is:

$$X_{CS}=\frac{\pi\left(\pi^2+4\right)}{8A}R_{\text{nom}} \tag{2}$$

The rated load power is:

$$P_{nom}=\frac{8}{\pi^2+4}\frac{V_{IN}^2}{R_{nom}}=\frac{1}{2}I_{nom}^2R_{nom} \tag{3}$$

The input voltage of the inverter can be expressed as:

$$V_{IN}=\frac{\sqrt{\pi^2+4}}{4}I_{\text{nom}}\,R_{\text{nom}} \tag{4}$$

where I_{nom} is the amplitude of the rated output current $i_{nom}(\omega t)$.

We assume that the output power is fully converted to the input power, i.e.:

$$P_{\text{nom}}=V_{\text{IN}}\cdot I_{\text{IN}}=\frac{1}{2}I_O^2R_O \tag{5}$$

The corresponding input current can be obtained as:

$$I_{\text{IN}}=\frac{2}{\sqrt{\pi^2+4}}\frac{R_O}{R_{\text{nom}}}\frac{I_O^2}{I_{\text{nom}}}=\frac{2}{\sqrt{\pi^2+4}}r_Oi_{\text{N}}I_O \tag{6}$$

where $r_O=R_O/R_{nom}$ is the normalized load resistance, and $i_N=I_O/I_{nom}$ is the normalized output current amplitude.

The voltage across the switching device is obtained as follows:

$$v_S(\omega t)=\begin{cases}0,\ 0\le\omega t<\pi\\ X_{CS}\int_{\pi}^{\omega t}(I_{IN}-i_O)d\omega\tau,\ \pi\le\omega t<\varphi_S\\ 0,\ \varphi_S\le\omega t<2\pi\end{cases} \tag{7}$$

where ϕ_S is the moment when the voltage across the switch drops to zero, i.e.:

$$v_S(\omega t=\varphi_S)=0 \tag{8}$$

From the voltage-second balance of the resonant inductor L_{CF}, it is obtained:

$$V_{IN}=\frac{1}{2\pi}\int_{\pi}^{\varphi_S}v_Sd\omega t \tag{9}$$

$$I_O=\frac{|V_{S1}|}{|R_O+X_F+X_O|}==\frac{\sqrt{V_{S1R}^2+V_{S1X}^2}}{R_{\text{nom}}\sqrt{r_O^2+(x_F+x_O)^2}} \tag{10}$$

where $x_F=X_F/R_{\text{nom}}$ and $x_O=X_O/R_{\text{nom}}$ are the normalized reactances at frequency f_s, V_{S1} is the amplitude of the fundamental component of the switching voltage V_S, and V_{S1R} and V_{S1X} are the Fourier series coefficients of V_{S1}. Then (11) can be obtained based on (8–10).

$$\begin{cases}\frac{i_{\text{N}}}{4A}\left(r_oi_{\text{N}}(\pi-\varphi_S)^2+\sqrt{\pi^2+4}((\varphi_S-\pi)\cos\varphi+\sin\varphi+\sin(\varphi+\varphi_S))\right)=1\\ \frac{2r_oi_{\text{N}}}{\sqrt{\pi^2+4}}(\varphi_S-\pi)+\cos(\varphi_S+\pi)+\cos\varphi=0\\ \left(\frac{\pi^2+4}{16A}\right)^2\times\left\{\left[\begin{array}{l}\frac{4r_oi_{\text{N}}}{\sqrt{\pi^2+4}}((\pi-\varphi_S)\cos\varphi_S+\sin\varphi_S)\\ +(\pi-\varphi_S)\sin\varphi-\cos(\varphi-\varphi_S)\\ -\cos(\varphi+\varphi_S)-\frac{1}{2}(3\cos\varphi+\cos(\varphi+2\varphi_S))\end{array}\right]^2+\left[\begin{array}{l}\frac{4r_oi_{\text{N}}}{\sqrt{\pi^2+4}}(1+\cos\varphi_S+(\varphi_S-\pi)\sin\varphi_S)\\ +(\varphi_S-\pi)\cos\varphi+\sin(\varphi+\varphi_S)-\sin(\varphi-\varphi_S)\\ -\cos(\varphi+\varphi_S)-\frac{1}{2}(3\cos\varphi+\cos(\varphi+2\varphi_S))\\ +\frac{1}{2}(\sin(\varphi+2\varphi_S)-\sin\varphi)\end{array}\right]^2\right\}=r_o^2+(x_F+x_o)^2\end{cases} \tag{11}$$

Figure 2 depicts the ZVS operating area corresponding to the normalized load resistance and reactance of the Class E inverter. At high frequency, the switching loss accounts for the main part of the system loss, so the ZVS working area of the inverter module can be equivalent to the efficient working area of the system. The switch turns

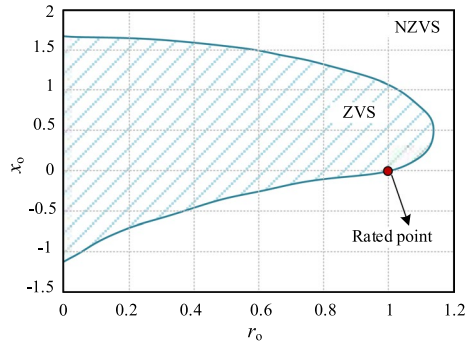

Fig. 2 Class E inverter ZVS operation area

on at time 2π, and the region that satisfies $\pi \le \phi_S \le 2\pi$ is the ZVS region, while the region satisfying $\phi_S = 2\pi$ is the rated optimal load of the inverter which can realize both ZVS and ZVDS, i.e., the boundary point depicted by the blue line in Fig. 2. The area corresponding to $\phi_S > 2\pi$ is the NZVS region, so when the load point falls to the NZVS area, the switch cannot realize soft switching. As the analysis shows, the ZVS region of the Class E inverter is related to the resonant inductor, capacitor and load as well as the duty cycle. Usually, the duty cycle is selected to be 0.5 as in this paper. When the ZVS condition is not required, the duty cycle of the switch can be slightly varied around 0.5. This will also affect the shape of the ZVS region.

2.2 Power combining network design

The power connection network with two modules connected in parallel is explored first, and the corresponding conclusions are then extended to any number of modules connected in parallel. Figure 3 is an equivalent circuit diagram of two inverter modules connected in parallel through a power synthesis network. The outputs of the inverter can be equivalent to sinusoidal voltage sources v_1 and v_2, and the L_P and C_P networks form a power synthesis module.

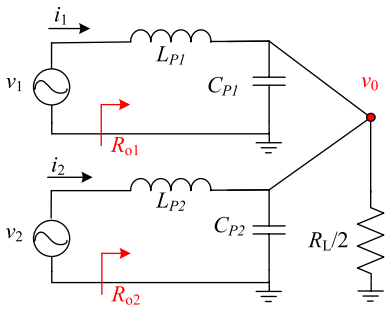

Fig. 3 Parallel combination circuit of two inverter modules

In Fig. 3, L_P and C_P form an L-type low-pass impedance matching network, which can convert the inverter output resistance R_O into the actual load R_L of the circuit which is larger than R_O, to achieve high power output. The capacitance and inductance required for impedance matching can be calculated by [22]:

$$\begin{cases} L_P = \frac{R_O}{\omega}\sqrt{\frac{R_L}{R_O} - 1} \\ C_P = \frac{1}{\omega R_L}\sqrt{\frac{R_L}{R_O} - 1} \end{cases} \tag{12}$$

The original output power of each inverter module is:

$$P_{1,\text{ori}} = P_{2,\text{ori}} = \frac{V^2}{2}\frac{1}{R_O} \tag{13}$$

Based on the direct power combination, another characteristic of equal power distribution is expected. In order to maintain the impedance matching function provided by the original low-pass matching circuit, the output power from the two voltage sources v_1 and v_2 need to be equal to the original output power of the traditional low-pass matching network.

Let $P_{1,\text{ori}} = P_1$, L_P and C_P can be obtained as:

$$\begin{cases} L_P = \frac{\sqrt{R_L R_O}}{\omega} \\ C_P = \frac{1}{\omega\sqrt{R_L R_O}} \end{cases} \tag{14}$$

The parameter design of L_P and C_P cannot guarantee that the equivalent impedance of the power synthesis network is resistive, so it is necessary to check whether the addition of the network will affect the soft switching performance of each inverter module. After the impedance matching network, the load of the inverter is not purely resistive, and the transformed input impedance is:

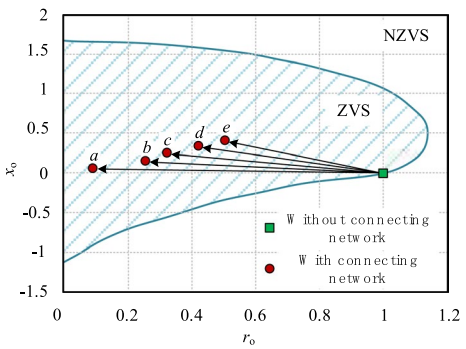

Fig. 4 Impedance moving direction after joining power combining network

$$Z_{IN} = \frac{R_O}{1+\frac{R_O}{R_L}}\left(1+j\sqrt{\frac{R_O}{R_L}}\right) = \frac{R_L}{\left(1+\omega^2 C_P^2 R_L^2\right)} + \frac{j\omega\left(L_P\left(1+\omega^2 C_P^2 R_L^2\right)-C_P R_L^2\right)}{1+\omega^2 C_P^2 R_L^2} \tag{15}$$

Figure 4 shows the change trend of the impedance of the system after adding the power connection network. When the reduced resistance ratio is 0.1, 0.3, 0.5, 0.7, 0.9, the equivalent impedance of the inverter module changes from (1, 0) points to *a, b, c, d, e*, respectively. This means that when the reduced resistance ratio is less than 1, after adding the power connection network, the equivalent impedance will fall in the ZVS working area, and thus will not affect the soft switching performance of the inverter module.

Therefore, L_P and C_P are designed according to (14). This can achieve maximum power capacity output and reduce the influence of multi-module connection on power variation with impedance matching, while the transformed impedance can also achieve ZVS.

3 Multi-module impedance analysis

The control strategy for the multi-module parallel inverter system is to achieve wide power output by switching (ON/OFF) and phase shift control. The power step is generated by the ON/OFF control of the module, and the phase shift control is used to eliminate the difference between the steps.

For MHz operating frequency, it is necessary to ensure that the inverter works in the soft switching state, i.e., the equivalent impedance of each module should fall in the efficient working area.

3.1 Impedance analysis of ON/OFF control

The module with the driving signal to the switch gate is called the ON module, and the module that applies 0 V to the gate and keeps the switch open is called the OFF module. The equivalent circuit of the OFF module is shown in Fig. 5. It has two working states of "rectifier" and "resonance", affected by the ratio of the number of ON modules to the total modules. Suppose that there are

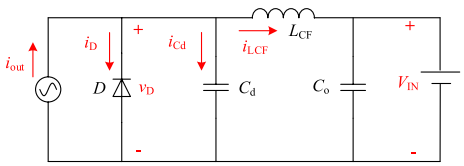

Fig. 5 Equivalent circuit of the "off" module

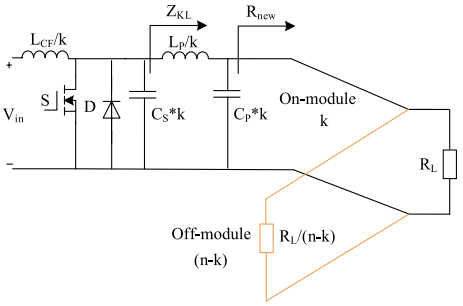

Fig. 6 Equivalent circuit when k is large

n total inverter modules in the system, of which *k* are ON modules and *n-k* are OFF modules.

When there are more ON modules, the output power is larger and the amplitude of the output AC voltage is also larger. The body diode *D* for the OFF module may conduct to transfer the energy to the input side, which is equivalent to connecting a DC voltage rectifier to the load. In this case, the OFF module is in the rectification state.

When the (*n-k*) OFF modules that are turned off work as inverters, the equivalent load of the corresponding output is $R_L/(n-k)$. Therefore, when it works as a rectifier, it can be equivalent to a load with resistance value of $R_L/(n-k)$, as shown in Fig. 6.

A new equivalent load impedance is obtained:

$$Z_{\mathrm{KL}} = k\cdot\left(jwLp + \frac{Rnew}{1+jwRnewCp}\right) \tag{16}$$

where

$$R_{\mathrm{new}} = R_L // \frac{R_L}{(n-k)} = \frac{R_L}{(n+1-k)} \tag{17}$$

Since the output power is proportional to the load resistance, when the equivalent electrical group becomes R_{new}, the output power of the inverter module is:

$$P_k = P_{\max}\times\frac{Z_{\mathrm{KL}}}{n\cdot R_{\mathrm{L}}} \tag{18}$$

where $P_{\max}$ is the full power output when all *n* modules are turned on. Part of the power in P_{k} will be fed back to the input side through the rectifier of the OFF module, and the actual power output to the load side is only $P_k\cdot R_{\mathrm{new}}/R_L$. In this case, the actual output power of the system is:

$$P_{\mathrm{out}} = \frac{P_k}{(n+1-k)} \tag{19}$$

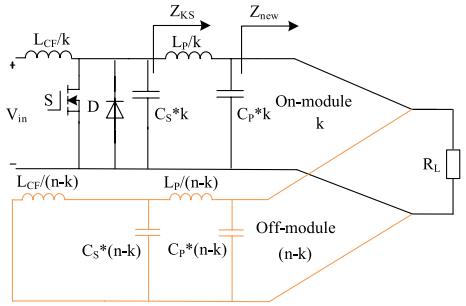

Fig. 7 Equivalent circuit when k is small

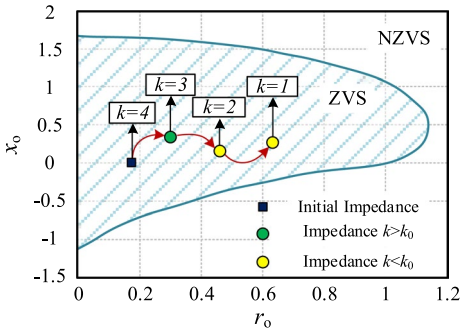

Fig. 8 Equivalent impedance movement track corresponding to the number of ON modules

As can be seen from (19), since the OFF modules work in the rectification state at this time, the switching control plays a large role in regulating system power.

When there are fewer modules, the output power is much less than the full power of the system, which means that the amplitude of the output AC voltage is greatly reduced, and the voltage across the diode is relatively small. The diode is connected to the DC input voltage through the inductor L_{CF}, so its voltage will fluctuate around this DC voltage. Once the amplitude of this fluctuating voltage is low enough, the minimum voltage across the diode will be higher than zero (diode becoming reverse biased), and the diode will no longer conduct. The equivalent circuit is shown in Fig. 7. It is in the "resonant" state of neither inverting nor rectifying. For each module there is an input capacitance which helps to maintain a constant input voltage. Figure 7 shows the diagram of the paralleled ON module and OFF module with high frequency AC. Because the input side voltage of the OFF module is a DC component, the input side can be seen as short-circuit under AC analysis.

At this time, the equivalent load impedance is:

$$Z_{KS} = k \cdot (jwLp + \frac{Znew}{1 + jwZnewCp}) \tag{20}$$

where

$$Z_{new} = \frac{R_L}{\left[\begin{array}{l} 1 - j\omega C_p R_L(n-k) + \\ \dfrac{j(n-k)R_L\left(1-\omega^2 L_{CF}C_s\right)}{\omega\left(L_p\left(1-\omega^2 L_{CF}C_s\right)+L_{CF}\right)} \end{array}\right]} \tag{21}$$

The critical point k_o of k value of "larger" and "smaller" number of ON modules is studied. We can specifically judge the working state of the OFF module and calculate the equivalent impedance of the system under the control of the switch.

As shown in Fig. 7, the OFF module is driven by the current source $i_{out}(\omega t) = I_{out}\sin(\omega t + \phi)$, where I_{out}, ω and ϕ are the current amplitude, angular frequency and initial phase angle, respectively. When the circuit works in the forward inverter state, the voltage resonates to 0 at the moment of switching on and zero voltage switching on (ZVS) can be realized. From the duality of the circuit, since working as a reverse rectifier, the current should resonance back to zero at the moment of switching off the diode and zero current switching off (ZCS) can be realized. When the diode is turned off, the differential equation can be written according to KCL and KVL:

$$\frac{d^2 v_D}{dt^2} + \frac{v_D}{L_{CF}C_S} - \frac{\omega L_{CF} I_{\text{out}} \cos(\omega t + \varphi) - V_{IN}}{L_{CF}C_S} = 0 \tag{22}$$

The solution is given as:

$$\begin{aligned} v_D(t) = {} & \frac{I_{out}}{C_S} \cdot \frac{\left[\begin{array}{l}(\omega \sin \omega t - \omega_d \sin \omega_d t)\sin\varphi \\ +\omega(\cos\omega_d t - \cos\omega t)\cos\varphi\end{array}\right]}{\omega^2 - \omega_d^2} \\ & - \frac{I_{out}}{C_S} \cdot \frac{\sin\omega_d t \sin\varphi}{\omega_d} + V_{IN}(1 - \cos\omega_d t) \end{aligned} \tag{23}$$

where $\omega_d = 1/\sqrt{L_{CF}C_S}$.

If the circuit works in the resonant state, the diode voltage is $v_{\text{DR}}(t) = v_{\text{D}}(t)$. If in the rectifier state, the diode voltage is:

$$v_{DC}(t) = \begin{cases} v_D(t), 0 \le t < DT \\ 0, DT \le t < T \end{cases} \tag{24}$$

From the voltage-second balance principle of the inductor L_{CF}, there are:

$$\frac{1}{T}\int_0^T v_D(t)dt = V_{IN} \tag{25}$$

$$I_{\text{out}} = \sqrt{\frac{P_{out}}{Z_{KL}}} \tag{26}$$

Based on the above equations, from the designed circuit parameters L_{CF} and C_S, as well as the system operating parameters T and V_{IN}, the critical point $ko = 2.08$ between the "rectification" and "resonance" states can be obtained for the prototype. That is, in the example here, the circuit works in the "resonance" state for $k = 1$, 2, whereas for $k = 3$, 4, the circuit operates in the "rectified" state.

Figure 8 shows the variation trend of the equivalent inverter impedance with different numbers of ON modules.

It can be seen that, from the parameters designed in this paper, with ON/OFF control, the equivalent impedance moves inside the ZVS area, that is, along the direction of the red arrow in Fig. 8. When switching control occurs, the value of equivalent impedance is related to the design of system parameters. Appropriate circuit parameters can enable the ON module to realize ZVS operation.

3.2 Phase shift mode control analysis

When phase shift control is adopted, the phase lag of output current will increase with the increase of phase shift angle. To achieve ZVS for the non-phase shift module, the equivalent impedance of the switch needs to be sensitive enough to completely discharge the junction capacitance of the switch. As the hysteresis angle of the output current increases, the inductive component of the equivalent load is enhanced, so ZVS can be well realized. However, for the phase shift module, with the increase of the phase shift angle, the phase of the output current may be ahead of the change of the V_{DS} voltage. In some phase shift ranges, the voltage and current during switching may overlap to a certain extent, resulting in the loss of the soft switching characteristic of the phase shift module.

For quantitative analysis, let the total number of modules be n and the number of ON modules be k, among which the number of non-phase shift modules is (k-r), the number of phase shift modules is r, and the phase shift angle is ϕ. As shown in Fig. 3, the output of the inverter module can be equivalent to a sinusoidal voltage source:

$$v_m = Ve^{j\omega t}(m = 1, ..., k - r) \tag{27}$$

$$v_n = Ve^{j(\omega t+\phi)}(n = k - r + 1, ..., k) \tag{28}$$

The actual load is connected in parallel with the OFF module to form a new impedance load Z_{newk}, and the output voltage is obtained as:

$$v_o = Ve^{j\omega t}\left(k - r + re^{j\phi}\right)\frac{Z_{newk}}{j\omega L_P} \tag{29}$$

When $k < k_o$ $Z_{newk} = R_{new}$, and when $k > k_o$, $Z_{newk} = Z_{new}$. The values of R_{new} and Z_{new} can be calculated using (17) and (21), respectively.

The output current of each module can be obtained as:

$$i_m = \frac{Ve^{j\omega t}}{j\omega L_P}\left(1 - \frac{\left(k - r + re^{j\phi}\right)Z_{newk}}{j\omega L_P}\right)(m = 1...k) \tag{30}$$

$$i_n = \frac{Ve^{j\omega t}}{j\omega L_P}\left(e^{j\phi} - \frac{\left(k - r + re^{j\phi}\right)Z_{newk}}{j\omega L_P}\right) \tag{31}$$

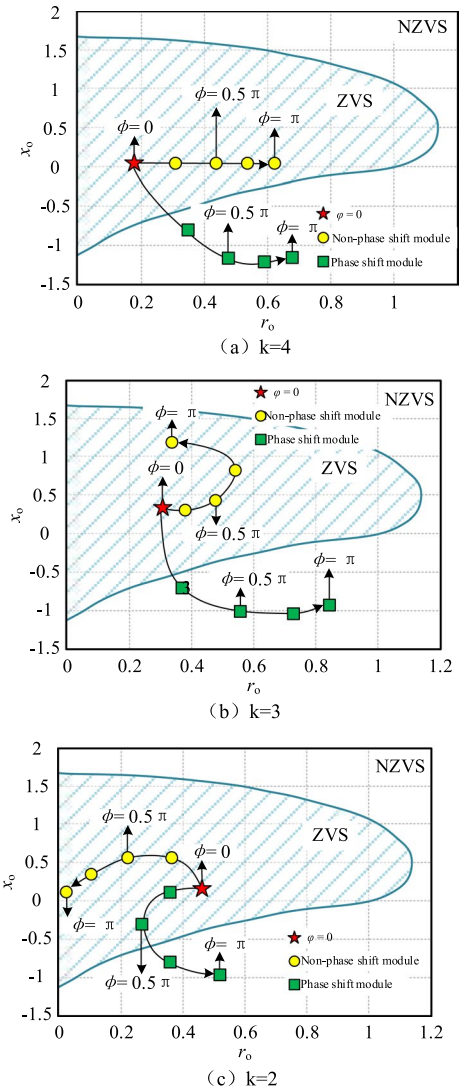

Fig. 9 Variation trends of equivalent impedance of non-phase shift module and phase shift module with different phase shift angles. **a** k = 4, **b** k = 3, **c** k = 2

The equivalent impedance of the non-phase shift module $Z_{k\text{-}r}$ and the equivalent impedance of the phase shift module Z_r are obtained as:

$$Z_{k-r} = \frac{v_m}{i_m} = \frac{j\omega L_P}{\left(1 - \frac{(k-r+re^{j\phi})Z_{newk}}{j\omega L_P}\right)} \tag{32}$$

$$Z_r = \frac{v_n}{i_n} = \frac{j\omega L_P e^{j\phi}}{\left(e^{j\phi} - \frac{(k-r+re^{j\phi})Z_{newk}}{j\omega L_P}\right)} \tag{33}$$

System output power can be expressed as:

$$\begin{aligned} P_{\text{out}} &= (k-r)\cdot \text{Re}\left[\frac{v_m i_m^*}{2}\right] + r\cdot \text{Re}\left[\frac{v_n i_n^*}{2}\right] \\ &= (k-r)\cdot \frac{V^2}{2}\text{Re}\left[\frac{1}{Z_{k-r}}\right] + r\cdot \frac{V^2}{2}\text{Re}\left[\frac{1}{Z_r}\right] \end{aligned} \tag{34}$$

Figure 9 shows the variation trends of the equivalent impedance of non-phase shift module and phase shift module with different phase shift angles. As shown, when the phase shift angle ϕ changes, the equivalent impedance of the non-phase shift module moves inside the ZVS working area, which ensures the realization of soft switching. However, the equivalent impedance of the phase shift module moves toward the NZVS work area with the change of the phase shift angle ϕ, and its changing relationship is complicated. In particular, when $k > k_o$, a small phase shift angle will take the phase shift module out of the ZVS region. Therefore, the number of phase shift modules in the system is designed to be one, which can minimize the decline of system efficiency.

4 Experimental verification

To verify the accuracy of the theoretical analysis and feasibility of the control strategy, a 13.56 MHz four-module inverter system is built, and the picture of the prototype is shown in Fig. 10.

The parameters are optimally designed considering the paralleled module effect previously analyzed. For the Class E inverter, the input resonant inductor $L_{\text{CF}} = 147$ nH and resonant capacitor $C_{\text{S}} = 400$ pF. In the design process, the switch output capacitance is fully adopted by the resonant capacitor, i.e., the value of discrete capacitance is the difference between the calculated value and the switch output capacitance. Thus, the switch output capacitance takes part in the resonance. This helps to reduce the value of the discrete capacitor. The design of the power connection module needs to meet the impedance matching requirement, and the load is 50 Ω. Since there are four modules in the circuit, the equivalent connection resistance of each module is 200 Ω. The

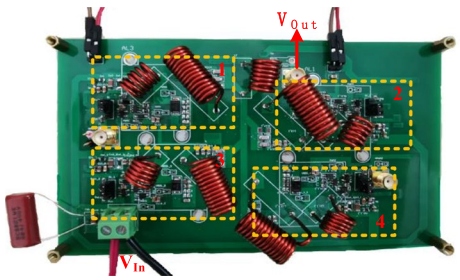

Fig. 10 High frequency multi-module inverter system prototype

Table 1 Key parameters and component types of the prototype

Parameters	Value (Model)
Switch S	GS61008T
Driver IC	LM5114
Parallel diode D	SS10100B
Logic AND Gate	NC7SZ08M5X
Input capacitance /μF	10
DC isolation capacitance C_B/nF	2
Resonant inductance L_{CF}/nH	147
Resonant capacitance C_S/pF	250
Matching inductance L_p/nH	475
Matching capacitance C_p/pF	300
Filter inductance L_0/nH	208.7
Filter capacitor C_{L2}/pF	660

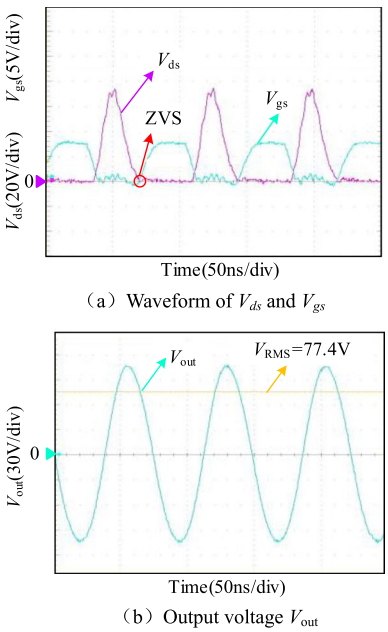

Fig. 11 Working waveforms under full power operation. **a** Waveform of V_{ds} and V_{gs} **b** Output voltage V_{out}

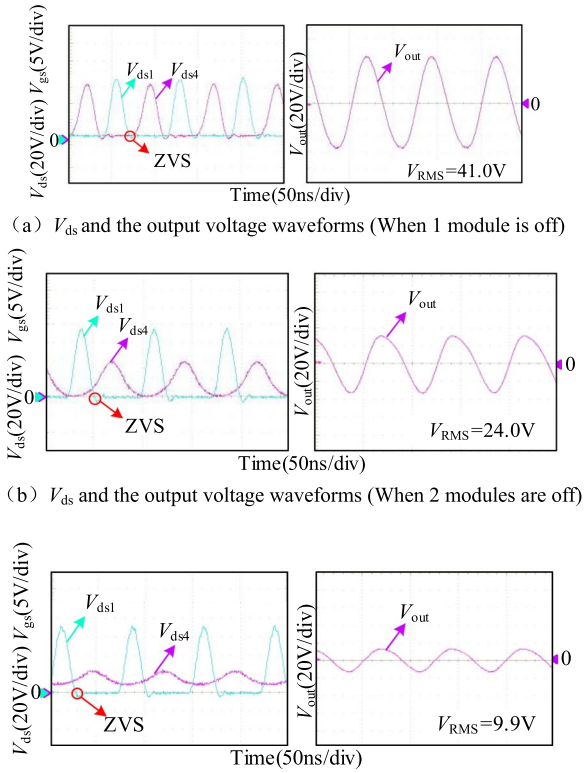

Fig. 12 System working waveforms under on–off control. **a** V_{ds} and the output voltage waveforms (When 1 module is off). **b** V_{ds} and the output voltage waveforms (When 2 modules are off). **c** V_{ds} and the output voltage waveforms (When 3 modules are off)

parameters of the power connection module can thus be calculated. The main parameters and device models of the prototype are shown in Table 1.

The system is tested at full power under rated working conditions first, and the main working waveforms of the inverter system are shown in Fig. 11. It can be seen that the system can achieve ZVS at full power. The input power is 133 W, the output voltage is $V_{P\text{-}P}$ = 219 V, the output power is 120 W, and the overall efficiency is 90.2%.

Next, the output power of the system is adjusted, and Fig. 12 shows the working waveforms when the system operates with different numbers of ON modules. As can be seen from the V_{ds} waveform, the switch of the ON module can always realize ZVS. When 1 module is off, as shown in Fig. 12a, the OFF module works in the rectification state. When 2 or 3 modules are off, as shown in Figs. 12 b and c, the lowest diode voltage (i.e. V_{ds}) is higher than zero (i.e., the diode is always reverse biased), and the diode cannot be turned on, so the OFF module works in resonance state.

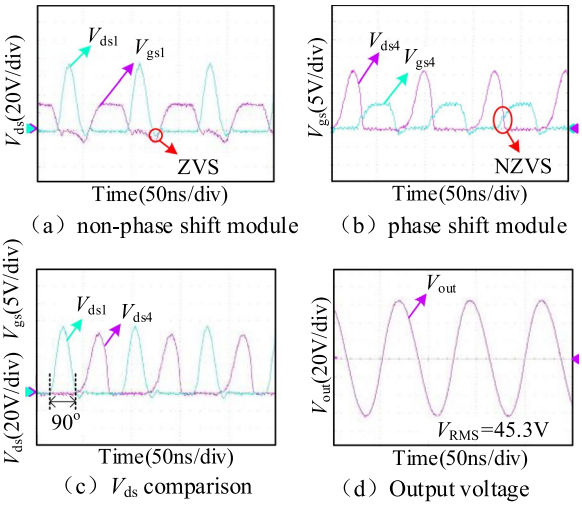

Fig. 13 Working waveforms with phase shift of 90°

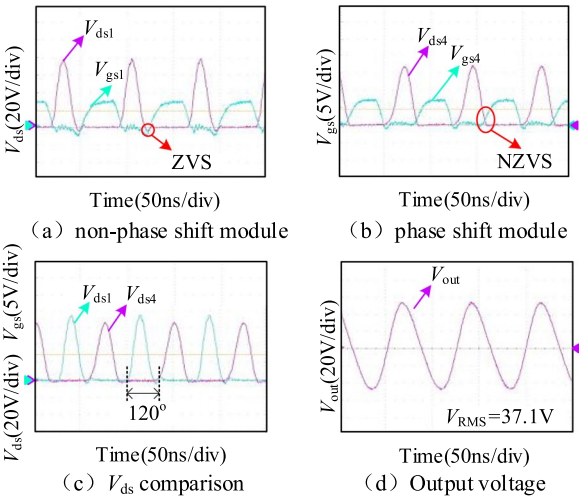

Fig. 14 Working waveforms with phase shift of 120°

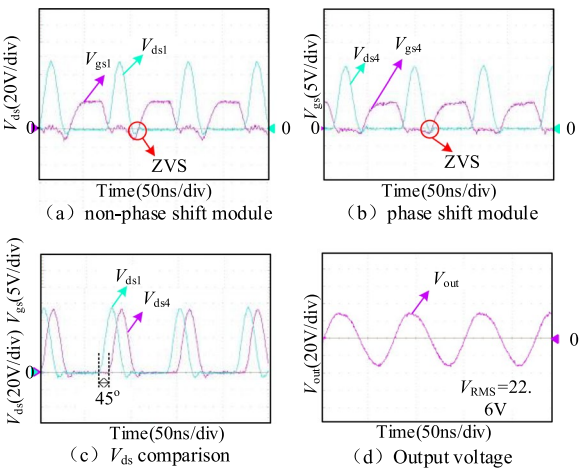

Fig. 15 Waveforms with two OFF modules and phase shift of 45°

When the number of ON modules of the prototype changes between 1–2-3–4, the corresponding output power varies as 1.96 W-11.6 W-33.7 W-120 W, and thus a wide range can be achieved. When other conditions are unchanged, the higher the number of ON modules, the greater the output power value.

Phase shift control is adopted in module 4, and the output power is further adjusted by combining the ON/OFF control of modules 1–3. Figures 13 and 14 show the system working waveforms under 90° and 120° phase shifts of module 4, while module 1, 2 and 3 are all on. In this case, the non-phase shift module can realize ZVS soft switching, while V_{ds} of the phase shift module cannot resonate to zero before the switch is turned on, so soft switching cannot be realized. When the phase shift angle changes, the system output power also changes. When the module phase shifts by 0°–90°–120°, the corresponding output power P_{out} varies as 120 W-41.0 W-27.6 W.

Figure 15 shows the system working waveforms under 45° phase shift of module 4, while module 1 is on and modules 2 and 3 are off. The output power of the system is 10.2 W and the output voltage is $V_{P\text{-}P}=64$ V. At this time, the OFF module is dominant, and both the non-phase shift module and phase shift module work in the ZVS state. This is consistent with previous theoretical analysis.

For these different operating modes, the system efficiency is tested. With the optimal parameter design, the RF inverter efficiency is improved by more than 5% over the traditional parameter design method without considering the effect of the paralleled modules.

5 Conclusion

In this paper, the parameters of the proposed multi-module inverter system are designed, and the load impedance range of the Class E single-module inverter circuit is derived. The equivalent impedance and operating mode of the system are analyzed when ON/OFF control and phase shift control are adopted. The system efficiency can reach 90.2% at full power, and efficiency is improved by more than 5% when compared with the traditional parameter design method without considering the effect of the paralleled modules. The system ensures efficient operation while realizing a wide power output range.

Acknowledgements
Not applicable

Author contributions
TY analyzed the soft-switching operating range, impedance effect and interconnection relationship between the inverter modules, and was a major contributor in writing the manuscript. YG and WW performed the organization of the manuscript and were minor contributors in writing the manuscript. All authors read and approved the final manuscript.

Funding
The manuscript is funded by National Natural Science Foundation of China under grant 52007041.

Availability of data and materials
All data generated or analysed during this study are included in this published article.

Declarations

Competing interests
The authors declare that they have no known competing financial interests or personal relationships that could have appeared to influence the work reported in this paper.

Received: 29 November 2022 Accepted: 24 February 2023
Published online: 14 March 2023

References

1. Dixon, S., Dedrick, J., Charles, C., Gans, T., O'Connell, D., & Boswell, R. (2014). Phase resolved imaging of a repetitive extrusion of hydrogen plasma from a hollow cathode source. *IEEE Transactions on Plasma Science, 42*(10), 2834–2835.
2. Barnat, E. V. (2008). Structure in RF hydrogen plasma induced by magnetic field. *IEEE Transactions on Plasma Science, 36*(4), 1362–1363.
3. K. S. Kim, J. H. Seo, J. S. Nam, W. T. Ju, K. H. Paek and S. H. Hong, "Production of hydrogen and carbon black by methane decomposition using DC-RF hybrid thermal plasmas," The 31st IEEE international conference on plasma science, 2004, Baltimore, USA, 2004, pp. 220–226.
4. J. L. Giuliani, A. E. Robson, V. Shamamian and R. Campbell, "On the plasma extent in an RF inductively coupled, cylindrical, hydrogen discharge." 25th anniversary, IEEE conference record - abstracts. 1998 IEEE international conference on plasma science , Raleigh, USA, 1998, pp. 219–220.
5. J. Williams and M. Gundersen, "Variable density, uniform hydrogen plasma source for plasma-based accelerators." 2017 IEEE international conference on plasma science (ICOPS), USA, 2017, pp. 1–1.
6. F. J. Spiess, S. L. Suib, K. Irie, Y. Hayashi and H. Matsumoto, "Hydrogen production by water and methane plasma decomposition." IEEE conference record - abstracts. 2002 IEEE international conference on plasma science, Canada, 2002, pp. 255–260.
7. Donnelly, V. M., & Economou, D. J. (2011). *U.S. Patent Application No. 12/966,844*.
8. Dianguo, Xu., Leshi, G., Yijie, W., et al. (2016). Summary of research on ultra high frequency power converters. *Transactions of China Electrotechnical Society, 31*(19), 26–36.
9. Aldhaher, S., Yates, D. C., & Mitcheson, P. D. (2018). Load-independent class E/EF inverters and rectifiers for MHz-switching applications. *IEEE Transactions on Power Electronics., 33*(10), 8270–8287.
10. Shaoteng, Z., Zhao Jinbin, Wu., Yuebao, M. L., & Chao, L. (2021). Research on soft switching technology of class E inverter for radio energy transmission based on self mutual inductance regulation. *Transactions of China Electrotechnical Society, 36*(21), 4558–4566.
11. Singh, G. D., & Nallam, N. (2020). An RF choke-less class E power amplifier. *IEEE Transactions on Circuits and Systems II: Express Briefs., 67*(11), 2422–2426.
12. E. Aggrawal and K. Rawat. Analysis and design of chireix outphasing switched mode power amplifier. 2018 IEEE MTT-S Latin America microwave conference (LAMC 2018). 2018:1–3.
13. Y. Zhu, Z. Cheng, Y. Chen and G. Liu. Design of a broadband chireix combiner based on class-F power amplifier. 2019 8th International symposium on next generation electronics (ISNE). 2019:1–3.
14. Aggrawal, E., & Rawat, K. (2018). Chireix outphasing switched mode power amplifier for wireless communication. *IEEE MTT-S International Microwave and RF Conference (IMaRC)., 2018*, 1–4.

15. Mannem, N. S., Huang, T.-Y., & Wang, H. (2021). Broadband active load-modulation power amplification using coupled-line baluns: a multi-frequency role-exchange coupler doherty amplifier architecture. *IEEE Journal of Solid-State Circuits., 56*(10), 3109–3122.
16. Perreault, D. J. (2011). A new power combining and outphasing modulation system for high-efficiency power amplification. *IEEE Transactions on Circuits and Systems I: Regular Papers, 58*(8), 1713–1726.
17. Cordero, A., Ruiz, M. N., Vegas, D., & García, J. A. (2021). Outphasing class-E/F2 power amplifier using a quadrature hybrid as non-isolating combiner. *IEEE Topical Conference on RF/Microwave Power Amplifiers for Radio and Wireless Applications (PAWR)., 2021*, 1–4.
18. Zhang H, Bastami A, Jurkov A S, et al. Multi-Inverter Discrete Backoff: A high-efficiency, wide-range RF power generation architecture. 2020 IEEE 21st Workshop on control and modeling for power electronics (COMPEL). 2020.
19. Surakitbovorn, K., & Rivas-Davila, J. M. (2020). Modular ON/OFF and phase-shifting for high-speed radio frequency power modulation. *IEEE Open Journal of Power Electronics., 1*, 393–406.
20. Gurugubelli, V., Ghosh, A., & Panda, A. K. (2022). Parallel inverter control using different conventional control methods and an improved virtual oscillator control method in a standalone microgrid. *Protection and Control of Modern Power Systems, 7*(1), 1–13.
21. Azab, M. (2021). High performance decoupled active and reactive power control for three-phase grid-tied inverters using model predictive control. *Protection and Control of Modern Power Systems, 6*(3), 311–329.
22. Besser, L., & Gilmore, R. (2002). Practical RF circuit design for modern wireless systems: passive circuits and systems passive circuits and systems (Artech house microwave library), vol. 1, USA: Artech House.